Soft Matter

Jammed packings of 3D superellipsoids with tunable packing fraction, contact number, and ordering

Journal:	*Soft Matter*
Manuscript ID	SM-ART-09-2019-001932.R1
Article Type:	Paper
Date Submitted by the Author:	30-Oct-2019
Complete List of Authors:	Yuan, Ye; Peking University, College of engineering VanderWerf, Kyle; Yale University, Physics Shattuck, Mark; City College of New York, Benjamin Levich Institute and Physics Department O'Hern, Corey; Yale University, Mechanical Engineering

SCHOLARONE™
Manuscripts

Soft Matter

Jammed packings of 3D superellipsoids with tunable packing fraction, coordination number, and ordering[†]

Ye Yuan,[a,b] Kyle VanderWerf,[c] Mark D. Shattuck,[d] and Corey S. O'Hern[*,b,c,e,f]

We carry out numerical studies of static packings of frictionless superellipsoidal particles in three spatial dimensions. We consider more than 200 different particle shapes by varying the three shape parameters that define superellipsoids. We characterize the structural and mechanical properties of both disordered and ordered packings using two packing-generation protocols. We perform athermal quasi-static compression simulations starting from either random, dilute configurations (Protocol 1) or thermalized, dense configurations (Protocol 2), which allows us to tune the orientational order of the packings. In general, we find that superellipsoid packings are hypostatic, with coordination number $z_J < z_{\rm iso}$, where $z_{\rm iso} = 2d_f$ and $d_f = 5$ or 6 depending on whether the particles are axi-symmetric or not. Over the full range of orientational order, we find that the number of quartic modes of the dynamical matrix for the packings always matches the number of missing contacts relative to the isostatic value. This result suggests that there are no mechanically redundant contacts for ordered, yet hypostatic packings of superellipsoidal particles. Additionally, we find that the packing fraction at jamming onset for disordered packings of superellipsoidal depends on at least two particle shape parameters, e.g. the asphericity $\mathscr{A}$ and reduced aspect ratio β of the particles.

1 Introduction

Athermal particulate materials, such as granular media, foams, and emulsion droplets, typically jam, or become solid-like with a non-zero static shear modulus when they are compressed to sufficiently large packing fractions.[1–4] Unwanted jamming occurs in many industrial processes, such as clogging in hopper flows,[5] and controlled jamming and unjamming has been used in robotics to grip soft, sharp, or fragile objects.[6] Further, unjamming in geological systems, such as landslides and earthquakes, causes significant financial and human loss.

Many prior studies have focused on jamming in model systems composed of frictionless, spherical particles. Disordered packings of frictionless, monodisperse spherical particles are isostatic at jamming onset with $z_J = z_{\rm iso}$ contacts per particle, where

$z_{\rm iso} = 2d_f = 6$ and $d_f = 3$ is the number of translational degrees of freedom for spheres, and with packing fraction at jamming onset $\phi_J \approx 0.64$.[1,2,7,8] Previous work has characterized the critical scaling of the structural and mechanical properties[1,9–11] and the anomalous vibrational density of states[12,13] of jammed packings of spherical particles.[4]

However, most athermal, particulate systems in industrial processes and in nature are composed of highly non-spherical particles.[14,15] In general, disordered jammed packings of non-spherical particles are hypostatic with coordination number $z_J < z_{\rm iso}$, where $z_{\rm iso} = 10$ or 12 for axisymmetric and non-axisymmetric particles, respectively.[16–19] Thus, disordered jammed packings can possess a range of coordination numbers, $6 \le z_J \le 12$, and packing fractions at jamming onset that depend on the shape of the constituent particles. In two spatial dimensions (2D), we showed recently that disordered packings generated via athermal, quasistatic compression for a wide variety of non-spherical shapes are mechanically stable, despite the fact that $z_J < z_{\rm iso}$.[20,21] The mechanical stability of hypostatic packings with N nonspherical particles in d spatial dimensions can be assessed by calculating the eigenvalue spectrum of the dynamical matrix for each packing. Hypostatic packings are mechanically stable because they possess $Nd_f - d$ positive eigenvalues (in periodic boundary conditions), which matches the number of nontrivial degrees of freedom in

[a] Department of Mechanics and Engineering Science, College of Engineering, Peking University, Beijing 100871, China; E-mail: yuanyepeking@pku.edu.cn
[b] Department of Mechanical Engineering and Materials Science, Yale University, New Haven, Connecticut 06520, USA.
[c] Department of Physics, Yale University, New Haven, Connecticut 06520, USA.
[d] Benjamin Levich Institute and Physics Department, The City College of New York, New York, New York 10031, USA.
[e] Department of Applied Physics, Yale University, New Haven, Connecticut 06520, USA.
[f] Graduate Program in Computational Biology and Bioinformatics, Yale University, New Haven, Connecticut 06520, USA.

the system. Some of the eigenvalues correspond to "quadratic" modes and the others correspond to "quartic" modes. For a given quadratic mode, when the packing is perturbed by displacing the particles by an amplitude δ along this eigenmode of the dynamical matrix, the total potential energy U increases by δ^2. In contrast, at the onset of jamming where $U \to 0$, U increases by δ^4 when the system is perturbed along a quartic mode.[20,22] We find that the number of quadratic modes is $N_2 = N z_J/2$ and the number of missing contacts below the isostatic value, $N d_f - d + 1$, matches the number of quartic modes of the dynamical matrix. This result indicates that all of the degrees of freedom in the hypostatic packings are indeed constrained. From the perspective of the potential energy landscape, a mechanically stable hypostatic packing corresponds to a local minimum, but near the minimum, the directions along the quartic modes are much flatter than along the quadratic modes. Moreover, we have shown in prior work that hypostatic packings of ellipses and ellipsoids possess nonzero shear moduli, but the scaling of the shear moduli with pressure is different from that observed for sphere packings.[20,23]

Given that jammed packings of non-spherical particles can occur over a wide range of coordination numbers and packing fractions, is it possible to *a priori* determine whether a system is jammed if we are only given its z and ϕ? For *disordered* packings of monodisperse spheres, we know that if $\phi > 0.64$ and $z > 6$, the packing is jammed. For disordered packings of convex-shaped particles in 2D, we found that the packing fraction at jamming onset can be collapsed approximately onto a master curve that depends only on the shape parameter $A = p^2/4\pi a$, where p is the perimeter and a is the area of the particle.[21] In 2D, $\phi_J \approx 0.84$ for $A = 1$, ϕ_J increases with A, reaching a peak near $A \approx 1.1$, and then decreases continuously with further increases in A. Results for ϕ_J have also been reported for packings of nonspherical particles in 3D, but separately for each family of shapes, e.g., ellipsoids,[17] spherocylinders,[18,24,25] and spheropolyhedra.[26] Here, we will address the question of whether there is a general relationship between the packing fraction at jamming onset and one or more particle shape parameters in packings of non-spherical particles in 3D.

Further, few studies have attempted to connect the coordination number to mechanical stability for *ordered* packings of non-spherical particles,[27,28] despite the fact that packings of monodisperse particles that deviate by less than 20% from perfect sphericity can possess significant translational and orientational order. In particular, does the relationship between the number of missing contacts below the isostatic value and number of quartic modes hold for ordered or partially ordered packings of non-spherical particles? One might expect that some of the "extra" contacts that occur in ordered packings may be mechanically redundant,[29] and therefore will not contribute to the packing's stability, resulting in a mismatch between the number of missing contacts and the number of quartic modes.

We investigate these questions by generating static packings of monodisperse, frictionless, superellipsoidal-shaped particles in 3D using numerical simulations.[30–33] We consider more than 200 different particle shapes by changing the shape parameters that define superellipsoids. For each packing, we determine ϕ_J, z_J, the

orientational order, and the eigenvalues and eigenmodes of the dynamical matrix. We carry out two packing-generation protocols. In Protocol 1, we jam the packing via athermal quasistatic compression,[1,22,34,35] starting from a random, dilute initial configuration of particles. In Protocol 2, we thermalize an unjammed configuration at an intermediate packing fraction before applying the same athermal quasistatic compression protocol (Protocol 1). We find that Protocol 1 generates globally disordered packings with a narrow distribution of jammed packing fractions and coordination numbers. Protocol 2, on the other hand, is able to generate packings of superellipsoidal particles with a wide range of orientational order.

We describe several key results. First, for disordered packings of superellipsoidal particles in 3D generated via Protocol 1, we show that the jammed packing fraction depends strongly on at least two shape parameters, instead of only one as we found for 2D.[21] In addition, we find that z_J, even in *ordered* packings of superellipsoids, determines mechanical stability. In particular, the number of quartic eigenmodes of the dynamical matrix matches the number of missing contacts relative to the isostatic value N_c^{iso} in ordered superellipsoid packings, as well as in disordered packings.

The article is divided into several sections. In Sec. 2, we review the definition of superellipsoids, describe the two packing-generation protocols we implement, and define the orientational order parameters we use to measure the degree of order in jammed packings. In Sec. 3, we present our key results. Finally, in Section 4, we summarize our results and discuss directions for future research. We also include three Appendices. In Appendix A, we show that we widely sample the two shape parameters that characterize the shape of superellipsoids. In Appendix B, we examine the *local* orientational order in superellipsoid packings. Finally, in Appendix C, we show the correlation between the average curvature of the particles at interparticle contacts and the coordination number for packings of superellipsoids.

2 Methods

In this section, we begin by defining the shape parameters for superellipsoids, and explain the wide variation in particle shape that is possible by tuning these parameters. Next, we describe our two protocols, the athermal Protocol 1, and the thermal Protocol 2, which we use to generate disordered and ordered jammed packings of these shapes, respectively. We then discuss calculations of the eigenvalues and eigenmodes of the dynamical matrix for superellipsoid packings to measure their mechanical response. Finally, we define the two order parameters that we use to quantify the orientational order in the packings.

2.1 Model of superellipsoidal particles

The surface of a superellipsodal particle located at the origin is defined by

$$|x/a|^{2p} + |y/b|^{2p} + |z/c|^{2p} = 1, \tag{1}$$

where a, b, and c ($a \le b \le c$) are the lengths of the semi-major axes, and p is the deformation parameter.[19,36] For superellipsoids, there are three independent parameters that control the
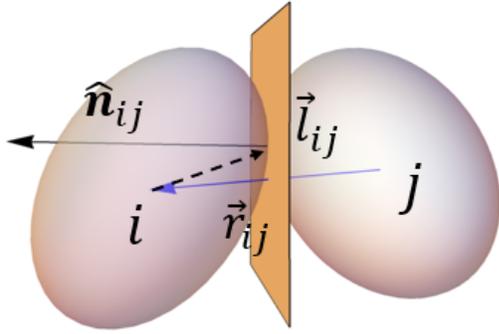
Fig. 1 Illustration of the simulation model for two contacting superellipsoids i and j. $\hat{n}_{ij}$ is the unit normal to the tangent plane at the point of contact (pointing toward particle i), $\vec{r}_{ij}$ is the center-to-center vector between particles i and j, and $\vec{l}_{ij}$ is the vector from the center of particle i to the point of contact between particles i and j.

particle shape, i.e., p and the two aspect ratios $w_1 = a/b$ and $w_2 = c/b$. If $a = b$, there is only one relevant aspect ratio $w = c/a$ and if $b = c$, $w = a/c$. Note that the particle shape reduces to a superball when $a = b = c$. By tuning p, we can vary the superellipsoid shape from ellipsoidal ($p = 1$) to octahedral ($p < 1$) and cuboidal ($p > 1$). We focus our studies on five specific p-values: $p = 0.75$, 0.85, 1, 1.5, and 2.

Instead of p and the aspect ratios, w_1 and w_2, the shape of superellipsoids can also be characterized by p, the reduced aspect ratio $\beta = ac/b^2$, and asphericity,

$$\mathcal{A} = 1 - (4\pi)^{1/3}(3V_p)^{2/3}/A_p, \qquad (2)$$

where V_p and A_p give the particle volume and surface area.[37,38] The shape parameter β allows us to distinguish "flattened" ($\beta < 1$) versus "elongated" ($\beta > 1$) shapes. The shape with $\beta = 1$ is termed a self-dual ellipsoid, which shows anomalous properties in disordered[17] and dense[39] packings. The asphericity satisfies $0 < \mathcal{A} < 1$, and $\mathcal{A} = 0$ for spheres. For the p values studied, the superellipsoidal particle shape in the β-$\mathcal{A}$ plane is roughly bounded by the values for prolate $\beta_{\max}(\mathcal{A})$ and oblate ellipsoids $\beta_{\min}(\mathcal{A})$ as shown in Fig. 12 in Appendix A. We focus on $\mathcal{A}$-values from 0 to ~ 0.35 and sample $\beta_{\min}(\mathcal{A}) < \beta < \beta_{\max}(\mathcal{A})$.

We consider pairwise, purely repulsive interactions between superellipsoids using the Perram and Wertheim formulation.[17,22,36,40,41]. For each pair of overlapping superellipsoids i and j, we calculate the volume scaling factor η_{ij} that brings the two superellipsoids to exact tangency. The potential energy for particles i and j is then defined by $U_{ij} = \varepsilon \zeta_{ij}^2/2$, where ε is the characteristic energy scale, $\zeta_{ij} = \eta_{ij}^2 - 1$, and $\eta_{ij} \leq 1$. The total potential energy is given by $U = \sum_{i>j} U_{ij}$. The repulsive force on particle i from j, $\vec{f}_{ij} = \vec{\nabla}_i U$, is given by

$$\vec{f}_{ij} = 2\varepsilon \zeta_{ij} \eta_{ij} \hat{n}_{ij}/(\vec{r}_{ij} \cdot \hat{n}_{ij}) \qquad (3)$$

where $\hat{n}_{ij}$ is the unit normal of the tangent plane between just-touching superellipsoids pointing toward i and $\vec{r}_{ij}$ is the center-to-center vector pointing from superellipsoid j to i. The torque $\vec{\tau}_{ij}$
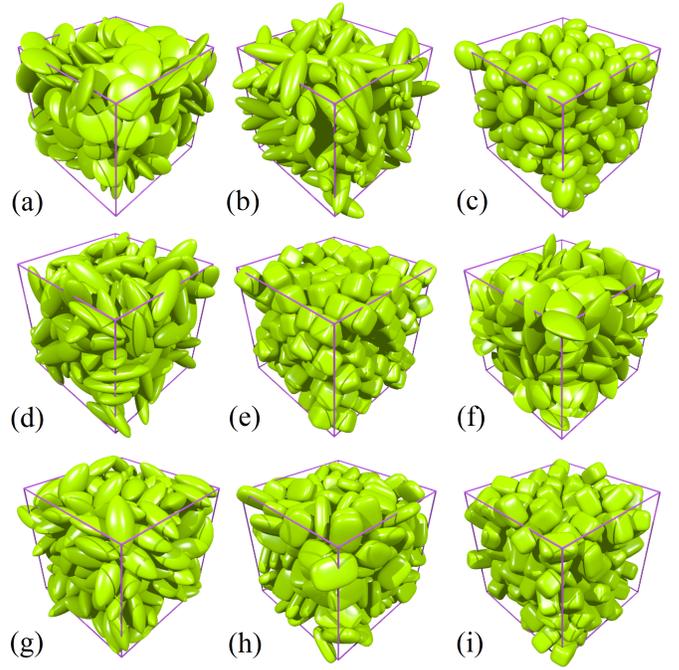

Fig. 2 Examples of nine static packings of superellipsoid particles with different shapes. The particle shape is characterized by (p, w_1, w_2): (a) oblate ellipsoid $(1, 0.3, 1)$, (b) prolate ellipsoid $(1, 1, 3)$, (c) self-dual ellipsoid $(1, 0.8, 1.25)$, (d) general ellipsoid $(1, 0.6, 2.36)$, (e) superball $(2, 1, 1)$, and four superellipsoids with (f) $(0.75, 0.4, 1)$, (g) $(0.85, 0.7, 2)$, (h) $(1.5, 0.5, 1.5)$, and (i) $(2, 1, 1.5)$.

on particle i from j is calculated using

$$\vec{\tau}_{ij} = \vec{l}_{ij} \times \vec{f}_{ij}, \qquad (4)$$

where $\vec{l}_{ij}$ is the vector from the center of particle i to the point of adjacency between superellipsoids i and j. See Fig. 1 for an illustration of $\hat{n}_{ij}$, $\vec{r}_{ij}$, and $\vec{l}_{ij}$ for two contacting superellipsoids. We will measure lengths, energies, and forces in terms of a, ε, and ε/a.

2.2 Packing-generation protocols

We generate jammed packings of $N = 400$ frictionless, monodisperse superellipsoidal particles in cubic simulation cells with periodic boundary conditions using two compression protocols: 1) an athermal protocol and 2) a thermal protocol. For Protocol 1, we first initialize an overlap-free, dilute configuration of particles with random positions and orientations. We then compress the configuration in small increments of packing fraction, $\Delta\phi = 10^{-3}$, minimizing the total potential energy U using the L-BFGS method[42] after each compression step. We terminate the energy minimization procedure at each compression step when the inter-particle overlaps are removed, achieving $U/N < U_{\text{tol}}$, where $U_{\text{tol}} = 10^{-10}$. We stop compressing the system when $U/N > U_{\text{tol}}$ and concurrently the average normalized force on a particle is below a small threshold, $\langle |\sum_j \vec{f}_{ij}| \rangle / \langle f_{ij} \rangle < \Delta$, where $\Delta = 10^{-4}$. We then measure the packing fraction ϕ_J, coordination number z_J, and other quantities of the first jammed packing with $U/N > U_{\text{tol}}$ that is closest to U_{tol}. We study the number of contacts in static
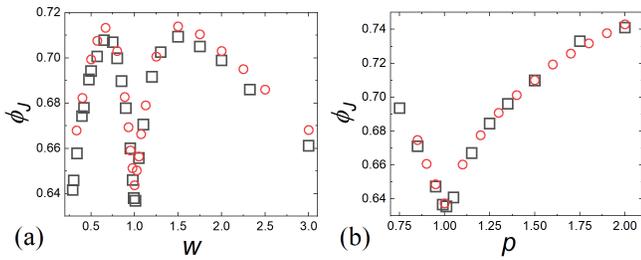
Fig. 3 (a) The packing fraction at jamming onset ϕ_J for packings of $N = 400$ prolate ($a = b$) or oblate ($b = c$) spheroids generated using Protocol 1 versus the aspect ratio w (open squares), as well ϕ_J for packings of spheroids from recent studies by Donev, *et al.* [17] (open circles). (b) ϕ_J for packings of superballs ($a = b = c$) generated using Protocol 1 versus the deformation parameter p, as well ϕ_J for packings of superballs from Jiao, *et al.* [19]

packings of nonspherical particles with force and torque balance on all non-rattler particles. We identify rattler particles as those with less than 4 interparticle contacts. Contacts are defined as nonzero overlaps between the two particles. The coordination number is defined as $z_J = 2N_c/(N - N_r)$, where N_c is the total number of contacts (excluding contacts from rattler particles) and N_r is the number of rattler particles. We find that the results presented here do not depend on the thresholds Δ and U_{tol}. Examples of nine static packings of superellipsoids with different shapes generated via Protocol 1 are shown in Fig. 2.

For Protocol 2, we first thermalize unjammed configurations at intermediate packing fractions $\phi_i \sim 0.55$, between the freezing and melting packing fractions for hard superellipsoids, [36,43] using Monte Carlo methods that do not allow particle overlaps for N_s steps. We then input these configurations into the compression and energy minimization procedure described in Protocol 1. By varying N_s and ϕ_i, we can obtain jammed packings of superellipsoids with tunable ϕ_J, coordination number z_J, and degree of orientational order.

To calculate average quantities for ϕ_J, z_J, and other quantities at jamming onset, we average over 5 to 10 independent initial conditions. We validated our methods for generating jammed packings of superellipsoids by comparing our results for ϕ_J from Protocol 1 to those from recent studies of packings of spheroids and superballs. [17,19] (See Fig. 3.)

2.3 Dynamical matrix

The dynamical matrix, which provides all possible second derivatives of the total potential energy with respect to the rotational and translational degrees of freedom of the system, determines the linear mechanical response of jammed particle packings. We define the dynamical matrix as

$$M_{kl} = \partial^2 U / \partial \xi_k \partial \xi_l, \tag{5}$$

where $\vec{\xi} = \{x_1, y_1, z_1, a\theta_1, a\phi_1, a\psi_1, \ldots, x_N, y_N, z_N, a\theta_N, a\phi_N, a\psi_N\}$, (x_i, y_i, z_i) is the location of the center of particle i, and $(\theta_i, \phi_i, \psi_i)$ are the rotation angles about the x-, y-, and z-axes used to define the orientation of particle i. Thus, the dimension of the dynamical matrix is $6N \times 6N$. For jammed superellipsoid packings

(in cubic simulation cells with periodic boundary conditions), the dynamical matrix possesses $6N' - 3$ nonzero eigenvalues λ_i (with corresponding unit eigenvectors $\hat{e}_i$), where $N' = N - N_r$ and N_r is the number of rattler particles with unconstrained translational or rotational degrees of freedom.

To determine M_{kl}, we calculated the first-order derivatives of the dynamical matrix, $\partial U / \partial \xi_k$ analytically, and calculated all of the the second-order derivatives numerically. We find that the eigenvalues of the dynamical matrix do not depend sensitively on the numerical derivatives for displacements $< 10^{-8}$.

2.4 Order parameters

In packings of non-spherical particles, one can measure the degree of order in the translational (i.e. positions of the particle centers) and rotational (i.e. orientations of the particles) degrees of freedom. In the systems we study, when the particle orientations are ordered, the particle positions also contain significant order. Thus, in these studies, we will focus on quantifying the orientational order.

We measure the global nematic S_2 [24,44] and cubic C_4 order parameters. [45] S_2 is defined as the largest eigenvalue of the 3×3 matrix:

$$S_{\alpha\beta} = \frac{3}{2} \langle \hat{s}_{\alpha i} \hat{s}_{\beta j} \rangle - \frac{\delta_{\alpha\beta}}{2} \tag{6}$$

where $\delta_{\alpha\beta}$ is the Kronecker delta, α, $\beta = x$, y, and z, $\hat{s}_{\alpha i}$ is the α-compoent of the unit vector that characterizes the orientation of particle i. and $\langle . \rangle$ indicates an average over all pairs of particles i and j. $\hat{s}_i$ is chosen as the shortest (longest) axis of the particle when $\beta < 1$ ($\beta > 1$). With this definition of $\hat{s}_i$, S_2 can capture stacking order that can occur in packings of flat shapes, as well as nematic order that can occur in packings of elongated shapes. $S_2 = 0$ for systems without orientational order and 1 for systems with complete particle alignment.

The cubic order parameter [45] C_4 is obtained by first calculating the fourth-order Legendre polynomial,

$$P_4(\hat{t}, \hat{u}_i) = \frac{1}{8} \left(35[\hat{t} \cdot \hat{u}_i]^4 - 30[\hat{t} \cdot \hat{u}_i]^2 + 3 \right), \tag{7}$$

where $\hat{t}$ is the unit vector aligned with one of the $3N$ orientations of the semi-major axes of each of the particles and $\hat{u}_i$ is a unit vector aligned with one of the three orientations of the semi-major axes for particle i. For each particle i in a given jammed packing, we select the $\hat{u}_i$ that maximizes $P_4(\hat{t}, \hat{u}_i)$ for a given $\hat{t}$. We then average $P_4^{max}(\hat{t})$ over all particles for a given $\hat{t}$ and define C_4 as the maximum over all $3N$ orientations $\hat{t}$. For $C_4 \sim 1$, packings possess large cubic order, which can occur in packings of cube-like particles with $p > 1$. In Appendix B, we show results for the local nematic and cubic order in packings of superellipsoids.

3 Results and Discussion

Our results are divided into two subsections. In Sec. 3.1, we present our results for disordered packings of superellipsoids generated via Protocol 1. We show the global nematic and cubic order parameters for packings containing a wide variety of superellipsoidal shapes. We find that the packing fraction at jamming onset for disordered packings of superellipsoids depends strongly
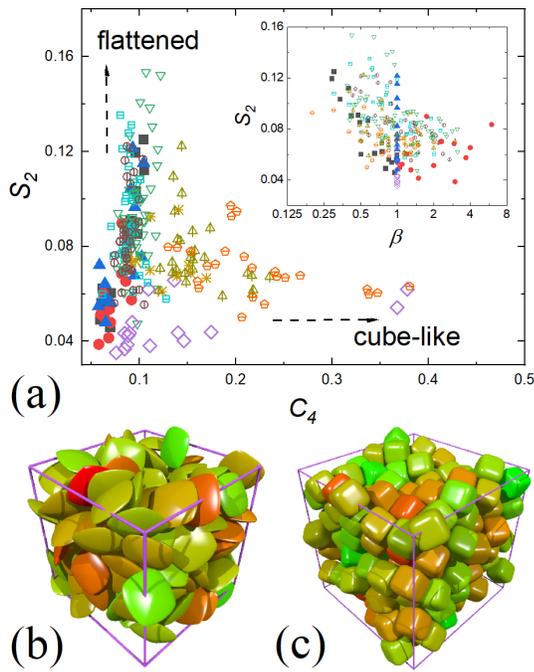
Fig. 4 (a) A scatter plot of the global nematic S_2 and cubatic C_4 order parameters for packings of superellipsoids generated via Protocol 1. The particle shapes include oblate ellipsoids (filled squares), prolate ellipsoids (filled circles), self-dual ellipsoids (filled upward triangles), general ellipsoids (downward open triangles), superballs (open diamonds), nearly spherical particles with $p \sim 1$ and $w \sim 1$ (asterisks), and $p = 0.75$ (squares with lines), 0.85 (circles with lines), 1.5 (upward triangles with lines), and 2.0 (pentagons with lines). The vertical (horizontal) arrow indicates packings with increasingly flatter (cube-like) shapes. The inset shows a scatter plot of S_2 versus the normalized aspect ratio β for the same data set. (b) Example packing of superellipsoids with $p = 0.75$ and $w = 0.3$ and global nematic order $S_2 = 0.11$. (c) Example packing of superballs with $p = 2$ and global cubatic order $C_4 = 0.37$. We show the (b) local nematic and (c) local cubatic order by coloring the particles with increasing local order from green to red.

on two shape parameters, $\mathscr{A}$ and β. In Sec. 3.2, we show that we can tune the packing fraction and coordination number at jamming onset by increasing the orientational order of the packings generated via Protocol 2. We also show that, even for ordered packings, the number of quartic modes of the dynamical matrix is equal to the isostatic number of contacts minus the number of contacts in the packing. Thus, we find a direct link between the coordination number and mechanical properties even for ordered packings of superellipsoids.

3.1 Disordered packings of superellipsoids

In this section, we focus on the structural propreties of superellipsoid packings generated via Protocol 1. In Fig. 4 (a), we show a scatter plot of the global nematic S_2 and cubatic C_4 order parameters for all jammed packings generated using Protocol 1. We find that many of the packings are disordered with S_2 and $C_4 \sim 1/\sqrt{N} \sim 0.07$. However, as demonstrated in the inset to Fig. 4 (a), S_2 increases as β decreases below 1 and the particle shape flattens. For more elongated shapes with $\beta > 1$, S_2 is roughly independent of β. We also find that the cubatic order increases as the
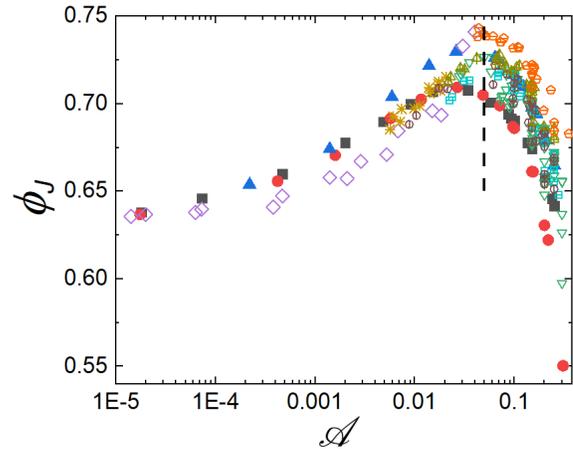

Fig. 5 The packing fraction at jamming onset ϕ_J versus the asphericity $\mathscr{A}$ for packings of the same shapes described in Fig. 4 generated via Protocol 1. The vertical dashed line marks the characteristic $\mathscr{A}_c \sim 0.05$ of the peak in the $\phi_J(\mathscr{A})$.

particles become more cube-shaped with $p > 1$, even though the packings were generated using the athermal protocol. In Fig. 4 (b) and (c), we show example packings of flattened and cube-like superellipsoids generated via Protocol 1 with elevated values of S_2 and C_4. In (b), we show the local nematic order of the particles for a packing of flattened superellipsoids with $p = 0.75$ and $w = 0.3$. In (c), we show the local cubatic order of the particles for a packing of superballs with $p = 2$. These packings possess local nematic and cubatic order. (See Appendix B.)

In Fig. 5, we show the packing fraction at jamming onset ϕ_J as a function of the asphericity $\mathscr{A}$ for a variety of superellipsoid shapes. The relation between ϕ_J and $\mathscr{A}$ is similar to that for packings of noncircular particles in 2D.[21] ϕ_J starts at a relatively low value for spherical particles (i.e. random close packing for monodisperse spheres with $\phi_J(0) \approx 0.64$), then grows with increasing asphericity, reaching a peak $\phi_J \sim 0.70$-0.74 near $\mathscr{A} \sim 0.05$, and then begins decreasing, falling below $\phi_J(0)$ for $\mathscr{A} > 0.1$. We also note that the data for $\phi(\mathscr{A})$ does not collapse as well onto a single curve in 3D, compared to the collapse of $\phi_J(\mathscr{A})$ for packings of 2D noncircular particles.[21]

In Fig. 6, we show the coordination number at jamming onset z_J versus the asphericity $\mathscr{A}$ for (a) spheroids with an axis of symmetry and $z_{iso} = 10$ and for (b) all other particle shapes with $z_{iso} = 12$. $z_J = 6$ for isostatic packings of spherical particles in the limit $\mathscr{A} \to 0$. As found previously, z_J for packings of nonspherical particles does not jump discontinuously from 6 to z_{iso} when $\mathscr{A}$ increases above zero. Instead, z_J increases continuously with $\mathscr{A}$. z_J for some of the particle shapes reaches z_{iso} for $\mathscr{A} < 0.35$, e.g. oblate, prolate, self-dual, and general ellipsoids, but others, such as superellipsoids with $p = 0.75$, 0.85, 1.5, and 2.0 do not. Note that z_{iso} is smaller for spheroids, compared to z_{iso} for other non-axisymmetric particle shapes, and thus the maximum packing fraction for spheroids is smaller than that for the other shapes we studied. We correlate values of $z_J < z_{iso}$ for superellipsoids with the surface curvature at interparticle contacts in Appendix C.

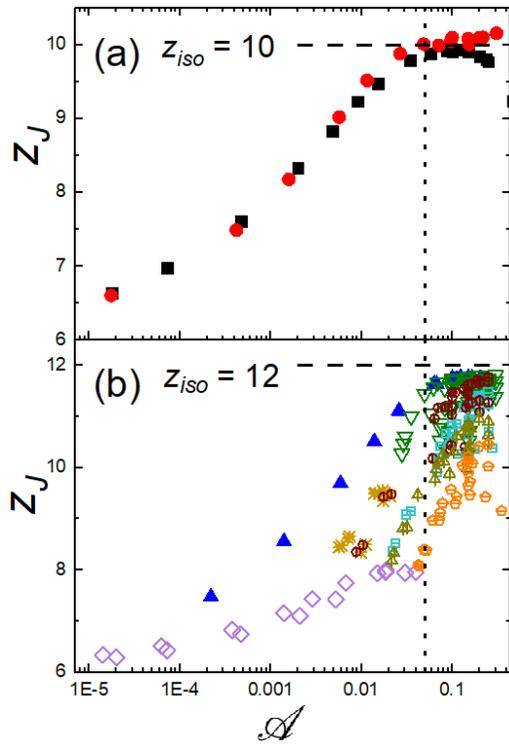The packing fraction at jamming onset ϕ_J for packings of su-

Fig. 6 The coordination number at jamming onset z_J versus asphericity $\mathscr{A}$ for packings generated via Protocol 1 for (a) spheroids and (b) all other shapes. The symbols are the same as those used in Fig. 4. The horizontal dashed lines in (a) and (b) indicate $z_{\text{iso}} = 10$ and 12 for the respective families of shapes. The vertical dotted line marks the threshold in $\mathscr{A} \sim 0.05$ above which $z_J(\mathscr{A})$ reaches a plateau for spheroids.

Fig. 7 (a) Packing fraction at jamming onset ϕ_J versus the reduced aspect ratio β for packings of superellipsoids generated using Protocol 1. The plot includes ellipsoids with four values of the asphericity $\mathscr{A} = 0.1$, 0.15, 0.2, and 0.25 and two families of superellipsoids with $p = 0.75$ (se0.75) and 0.85 (se0.85). (b) Contour plot of ϕ_J as a function of $\mathscr{A}$ and β. The horizontal dashed line indicates $\beta = 1$.

perellipsoids does not completely collapse when plotted versus a single shape parameter, *e.g.* the asphericity $\mathscr{A}$. (See Fig. 5.) This result suggests that ϕ_J for packings of nonspherical particles in 3D depends on two or more shape parameters. In Fig. 7 (a), we show ϕ_J versus the reduced aspect ratio β for several values of the asphericity $\mathscr{A} = 0.1$, 0.15, 0.2, and 0.25, excluding cube-like superellipsoids with $p > 1$. All of the curves $\phi_J(\beta)$ are concave down for the different values of $\mathscr{A}$. In Fig. 7 (b), we show a contour plot of ϕ_J as a function of both β and $\mathscr{A}$. We find that at small $\mathscr{A}$, the largest ϕ_J, ϕ_J^{max}, occurs near $\beta = 1$, however, ϕ_J^{max} shifts to $\beta > 1$ when $\mathscr{A} > 0.2$. Thus, ϕ_J depends on both shape parameters $\mathscr{A}$ and β.

3.2 Tunable hypostaticity

In this section, we show that we can increase the nematic or cubatic order in packings of superellipsoids using Protocol 2 to generate the packings. We compare ϕ_J and z_J at jamming onset for packings generated via Protocols 1 and 2. We focus on packings of superballs with $p = 1.25$ and 1.5 and packings of oblate ellipsoids with $w = 0.3$.

In Fig. 8 (a), we show the global nematic S_2 and cubatic C_4 order parameters versus the packing fraction at jamming onset ϕ_J for single packings of oblate ellipsoids (with $w = 0.3$) and superballs (with $p = 1.25$ and 1.5) generated via Protocol 2. We also
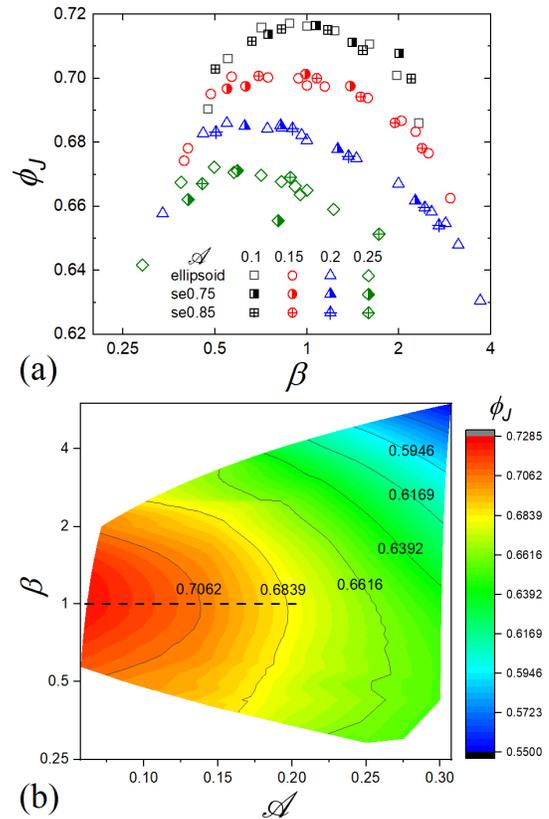
compare these results to those for packings of the same shapes, but generated using Protocol 1. Example packings are displayed in Fig. 8 (b). We find that S_2 and $C_4 < 0.1$-0.2 for packings generated via Protocol 1. However, S_2 and C_4 can become larger than 0.7 for packings generated using Protocol 2. For all shapes studied, ϕ_J increases with increasing orientational order.

In Fig. 9 (a), we show the eigenvalue spectrum of the dynamical matrix (Eq. 5) sorted from smallest to largest for packings of 6 different types of superellipsoids. As found in previous studies of packings of ellipsoids, the eigenvalue spectrum has three distinct regimes.[22] For a given eigenvector $\hat{e}_i$, the contribution of the translational degrees of freedom is defined by

$$T_i = \sum_{j=1}^{N} \sum_{\gamma} [\hat{e}_i]_{j\gamma}^2, \qquad (8)$$

where γ is summed over the three translational degrees of freedom x, y, and z for particles j in $\hat{e}_i$ and $T_i + R_i = 1$. In Fig. 9 (b), we find that in regime 3 ($i > 3N$), the eigenmodes are largely translational ($T_i \sim 1$). The T_i values in regime 2 for nearly spherical shapes (i.e. superballs with $p = 1.02$ and self-dual ellipsoids $w_1 = 0.98$) are small, indicating that the modes are largely rotational. As the asphericity increases, regimes 2 and 3 merge and
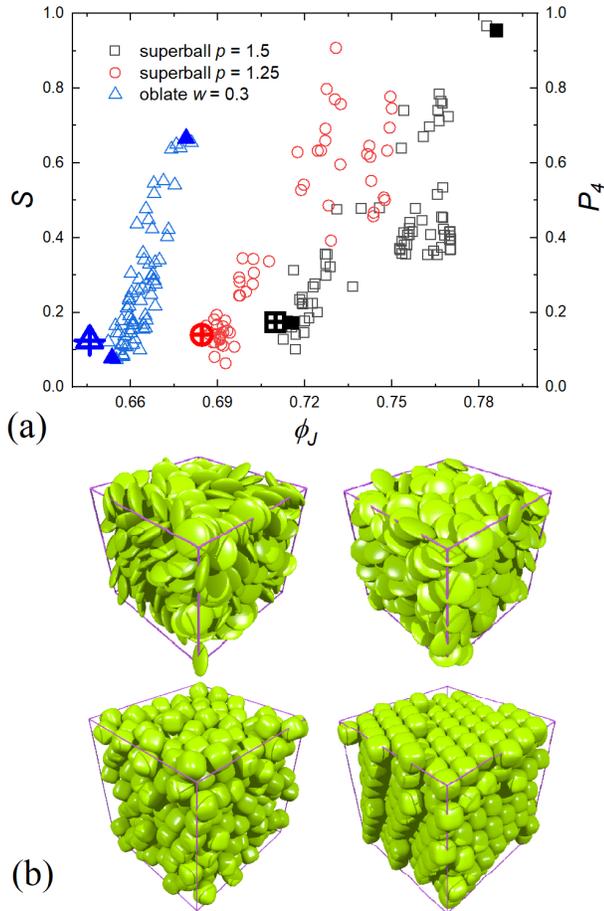
Fig. 8 (a) Global nematic S_2 (left axis) and cubic C_4 (right axis) order parameters for single packings of superballs ($p = 1.25$ and 1.5) and oblate ellipsoids ($w = 0.3$) generated using Protocol 2 are plotted versus ϕ_J. The average values of S_2 and C_4 for an ensemble of packings with the same particle shape, but generated using Protocol 1, are shown using corresponding symbols with crosses on the inside. The filled symbols represent the four packings shown in panel (b). (b) [top] Example packings generated via (left) Protocol 1 and (right) 2 for oblate ellipsoids with $w = 0.3$ and [bottom] example packings generated via (left) Protocol 1 and (right) 2 for superballs with $p = 1.5$.

Fig. 9 (a) Sorted eigenvalues λ_i of the dynamical matrix for packings of several shapes, including three types of superballs ($p = 1.02$, 1.15, and 1.5) and three types of self-dual ellipsoids ($w_1 = 0.98$, 0.9, and 0.6). Three distinct regimes of the spectrum are marked 1, 2, and 3. (b) The contribution of the translational degrees of freedom T_i to each eigenvector $\hat{e}_i$ for the same packings as in (a).

T_i increases. Quartic modes always correspond to the lowest frequency modes, and the translational content of these eigenmodes is small for nearly spherical particle shapes, and increases with asphericity.

When the system is perturbed along a quartic eigenmode $\hat{e}_i$ in regime 1, the change in the total potential energy ΔU between the unperturbed and pertrubed packings first increases quadratically with the perturbation amplitude δ, but then scales as δ^4 beyond a characteristic amplitude δ^* that scales to zero with decreasing pressure. (See the left of Fig. 10 (a).) We found in previous studies of nonspherical particles that the number of quartic modes N_q matches the deviation in the number of contacts at jamming onset from the isostatic value, i.e. $N_c = N_c^{\text{iso}} - N_q$, where $N_c^{\text{iso}} = d_f(N - N_r) - 2$. We show this result for packings of superellipsoids generated via Protocol 1 in Fig. 10 (b). This result emphasizes that even though $N_c < N_c^{\text{iso}}$, disordered packings of superellipsoids
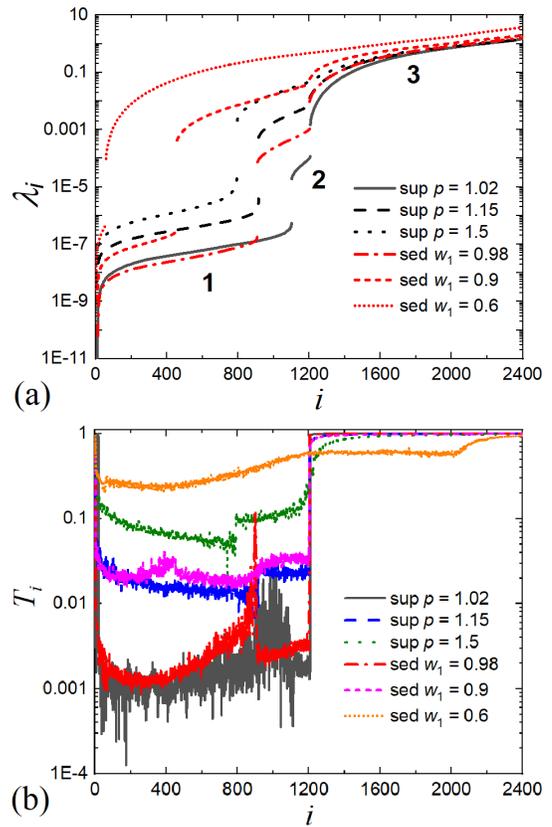
generated via Protocol 1 are mechanically stable.

Is the relationship between the number of contacts and number of quartic modes the same for packings of nonspherical particles with significant orientational order? For example, in ordered systems, it is possible that some of the N_c contacts are redundant and therefore do not provide independent constraints to block the degrees of freedom in the packings. In Fig. 11 (a), we show the z_J for packings of three types of superellipsoids generated via Protocol 2 that possess significant global nematic and cubatic order (*c.f.* Fig. 4 (a)). The coordination number in these systems ($z_J \to 10$) is much larger than that for packings generated using Protocol 1.

In Fig. 11 (b), we show the eigenvalue spectrum of the dynamical matrix for three packings of superballs with $p = 1.5$ generated using Protocol 2. As shown previously, the spectrum includes three regimes with a regime of quartic eigenmodes at the lowest values. Further, the crossover in behavior from $\Delta U \sim \delta^2$ to $\sim \delta^4$ occurs at a similar value of δ^* that scales to zero with decreasing pressure. (See the right panel of Fig. 10 (a).) In the inset of Fig. 11 (b), we show the number of contacts N_c versus the number of quartic modes N_q for all of the packings generated using Protocol 2. We find that even with significant orientational order, the number of quartic modes matches the deviation in the number of contacts from the isostatic value. Thus, we find that there are
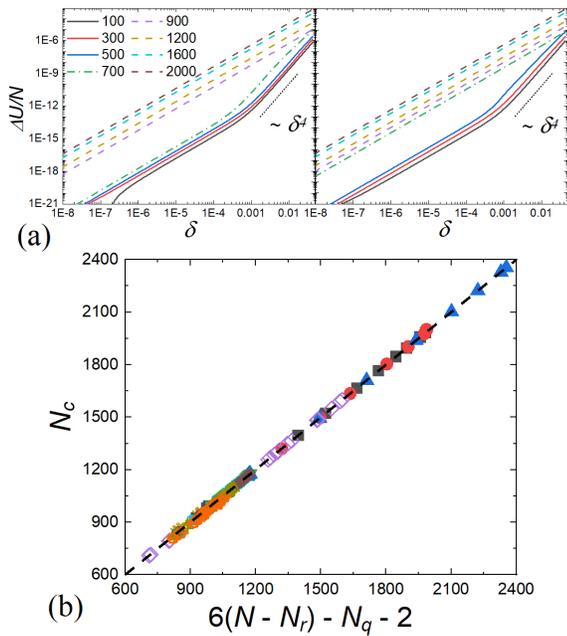
Fig. 10 (a) Change in the potential energy per particle $\Delta U/N$ between the perturbed and unperturbed packing for perturbations with amplitdue δ along several eigenmodes of the dynamical matrix for two packings of superballs with $p = 1.5$ and $z_J = 8.205$ (left) and 9.08 (right). $\Delta U \sim \delta^4$ at large δ for perturbations along the quartic eigenmodes (solid lines), whereas $\Delta U \sim \delta^2$ for perturbations along all other modes (dashed lines). (b) The number of contacts N_c versus $6(N - N_r) - N_q - 2$, where N_r is the number of rattler particles and N_q is the number of quartic eigenmodes for all the configurations in Figs. 5 and 6. The dashed line has unit slope and passes through the origin.

no redundant contacts for hypostatic packings of superellipsoids with $z_J < z_{\mathrm{iso}}$, and z_J determines their mechanical stability. In other words, the number of quadratic modes is consistently given by the number of existing contacts N_c, and the other degrees of freedom are constrained by the quartic modes.

4 Conclusions and Future Directions

In this article, we carried out computational studies of jammed packings of frictionless superellipsoids for more than 200 different particles shapes in three spatial dimensions. We implemented two protocols to generate static packings: Protocol 1, which uses athermal quasistatic compression, and Protocol 2, which includes thermal fluctuations and compression. Protocol 1 typically generates packings with small values of the global nematic and cubatic orientational order parameters, lower packing fraction ϕ_J and coordination number z_J at jamming onset. In contrast, Protocol 2 allows us to tune the orientational order (as well as ϕ_J and z_J) in packings of superellipsoids over a much wider range compared to those generated via Protocol 1.

We found several important results. Prior studies of disordered jammed packings of 2D nonspherical particles have shown that the packing fraction at jamming onset ϕ_J for a wide variety of shapes can be collapsed onto a masterlike curve with respect to a single shape parameter—the asphericity.[21] For disordered packings of superellipsoids in 3D, we find that two shape parameters, e.g. the asphericity $\mathscr{A}$ and reduced aspect ratio β, are required
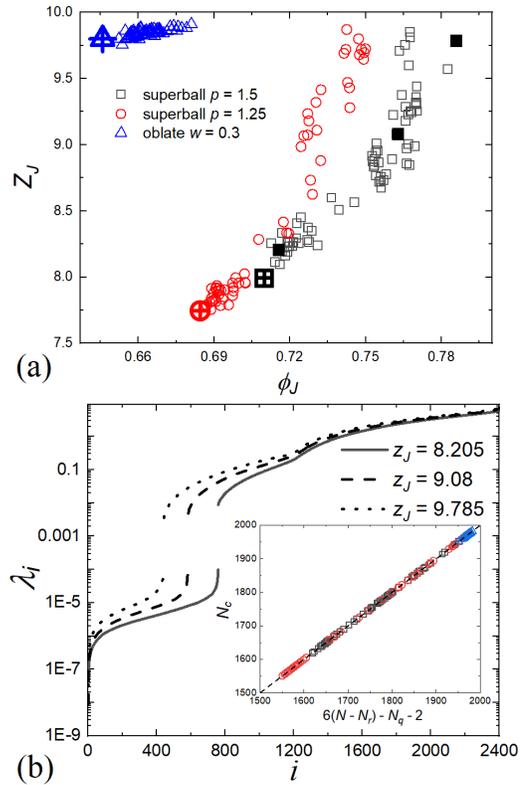

Fig. 11 (a) The coordination number at jamming onset z_J verus the packing fraction at jamming onset ϕ_J for the packings of superellipsoidal shapes considered in Fig. 8 generated via Protocol 2. Results for packings generated using Protocol 1 are represented by crosses. (b) Eigenvalues λ_i of the dynamical matrix sorted from smallest to largest for the three packings of superballs with $p = 1.5$ marked by the solid symbols in (a). The packings possess $z_J = 8.205$, 9.08, and 9.785. The inset shows N_c versus $N_c^{iso} - N_q$ for all packings of superellipsoids generated via Protocol 2. The dashed line has unit slope and passes through the origin.

to determine ϕ_J. Additionally, prior studies have found that packings of nonspherical particles are hypostatic with $z_J < z_{\mathrm{iso}}$, and the number of missing contacts below the isostatic value matches the number of quartic eigenmodes of the dynamical matrix.[20–22] Most of these prior studies have considered disordered packings of nonspherical particles with small values for global measures of orientational order. We find that the number of contacts $N_c = N_c^{iso} - N_q$, where N_c^{iso} is the number of contacts for an isostatic system and N_q is the number of quartic modes, for both disordered and ordered packings of nonspherical particles. The lack of redundant contacts implies that the number of quadratic modes is consistently given by the number of contacts N_c of the packing, and the other degrees of freedom are constrained by the quartic modes. If there were redundant contacts, we would observe packings with $N_c > N_c^{iso} - N_q$.

Our work opens up several new avenues of future research. First, in this work, we were able to generate packings of superellipsoids with tunable orientational order, ϕ_J, and z_J. However, we only considered packings with $z_J < z_{\mathrm{iso}}$. It will be interesting to generate packings of nonspherical particles with even more order, where $z_J > z_{\mathrm{iso}}$. In this case, do quartic modes still occur and if so, what determines their number? Another future research direction
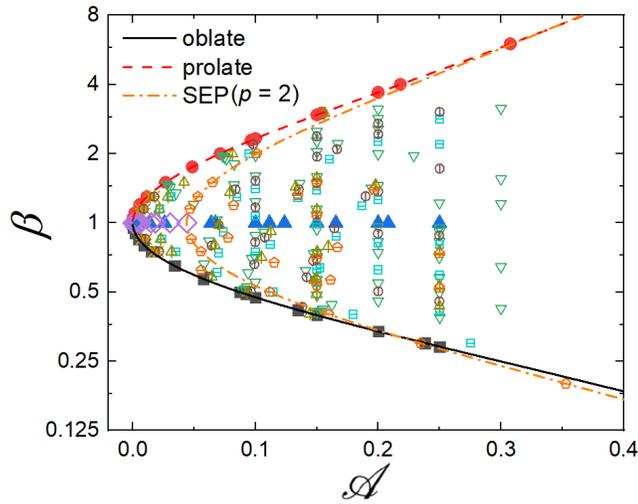
Fig. 12 The reduced aspect ratio β versus the asphericity $\mathscr{A}$ for all of the particle shapes studied. The solid and dashed curves correspond to Eqs. 9 and 10 for oblate and prolate ellipsoids, respectively. The dashed-dotted curve corresponds to superellipsoids with $p = 2$.

involves packings of *frictional* non-spherical particles.[46–50] Packings of frictional spherical particles can occur with coordination numbers that satisfy $d_f + 1 < z_J < 2d_f$, where $d_f = d$ for spherical particles.[51,52] Prior studies have shown that packings of frictional ellipsoids can possess $z_J \approx d + 1 = 4$.[46] Do these packings possess quartic modes, and if so, how many? It is clear that much more work is needed to understand the number of contacts that is required to determine the mechanical stability of packings of frictional, nonspherical particles.

Conflicts of interest

There are no conflicts to declare.

Appendix A: Variation of the shape parameters β and $\mathscr{A}$

In this Appendix, we show the range of reduced aspect ratio β and asphericity $\mathscr{A}$ that can be achieved for superellipsoidal particle shapes. For oblate and prolate ellipsoids, the asphericity $\mathscr{A}(\beta)$ can be written explcity. For oblate ellipsoids, we find

$$\mathscr{A}(\beta) = \frac{2\beta^{2/3}}{1 + \frac{\beta^2}{\sin\gamma}\ln\left(\frac{1+\sin\gamma}{\cos\gamma}\right)}, \qquad (9)$$

where $\gamma = \cos^{-1}\beta$. For prolate ellipsoids, $\mathscr{A}(\beta)$ can be expressed as

$$\mathscr{A}(\beta) = \frac{2\beta^{2/3}}{1 + \frac{\beta\alpha}{\sin\alpha}}, \qquad (10)$$

where $\alpha = \cos^{-1}\beta^{-1}$. In Fig. 12, we plot the relations between β and $\mathscr{A}$ for oblate and prolate ellipsoids, as well as $\beta(\mathscr{A})$ for superellipsoids with $p = 2$. We find that these curves serve as upper and lower bounds for the shape parameters of all other shapes that we study for $\mathscr{A} < 0.35$.
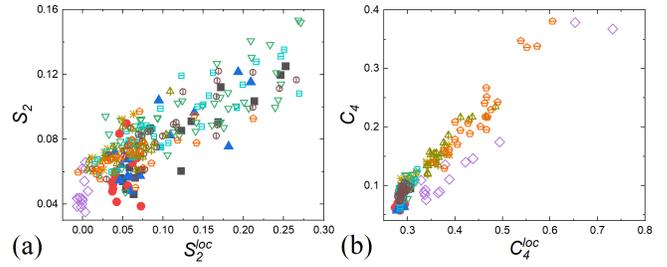

Fig. 13 (a) The global nematic order parameter S_2 plotted versus the local nematic order parameter S_2^{local} for all particle shapes studied. (b) The global cubatic order parameter C_4 plotted versus the local cubatic order parameter C_4^{loc} for all particle shapes studied.

Appendix B: Local nematic and cubatic order parameters

In the main text, for example in Figs. 4 (a) and 8 (a), we showed results for the global nematic S_2 and cubatic C_4 order parameters for packings of superellipsoids. In these figures, we also show example packings from the simulations with the particles colored according to the value of the local nematic and cubatic order parameters. The local nematic order parameter S_2^{loc} is defined analogously to Eq. 6 as the largest eigenvalue of the 3×3 matrix:

$$S_{\alpha\beta}^{\text{loc}} = \frac{3}{2}\left\langle \hat{s}_{\alpha i} \cdot \hat{s}_{\beta j}\right\rangle_j - \frac{\delta_{\alpha\beta}}{2}, \qquad (11)$$

where $\langle . \rangle_j$ averages over particles j that overlap particle i.

To define the local cubatic order parameter C_4^{loc} for particle i, we first calculate

$$P_4(\hat{u}_i, \hat{u}_j) = \frac{1}{8}\left(35[\hat{u}_j \cdot \hat{u}_i]^4 - 30[\hat{u}_j \cdot \hat{u}_i]^2 + 3\right), \qquad (12)$$

where $\hat{u}_j$ is a unit vector aligned with one of the three orientations of the semi-major axes for particle j that overlaps particle i. We first select the $\hat{u}_i$ orientation along one of the three semi-major axes that maximizes $P_4(\hat{u}_i, \hat{u}_j)$ for a given $\hat{u}_j$. We then average $P_4^{\text{max}}(\hat{u}_j)$ over all particles j that overlap i. The local cubatic order parameter C_4^{loc} is defined as the maximum over the three orientations for $\hat{u}_j$. We plot the global versus the local orientational order parameters in Fig. 13. For the nematic and cubatic order, the global and local order grow proprotionately.

Appendix C: Gaussian curvature at contact points

In this Appendix, we show that for packings of superellipsoids with small coordination numbers at jamming onset, the Gaussian curvature $\overline{K}_G$ at the points of contact are typically small, suggesting that two flat contacting surfaces can constrain multiple rotational degrees of freedom. In Fig. 14, we show the probability distribution $P(K_G)$, where $K_G = \overline{K}_G(abc)^{2/3}$, for superellipsoid packings generated via Protocol 1. (Note that each contact point contributes two K_G values.) We find that $P(K_G)$ for packings of cube-like superellipsoids, e.g. with $p = 2$ and small z_J, possesses a wide tail that extends to small values of K_G. For other particle shapes, such as oblate and prolate ellipsoids, $P(K_G)$ is much
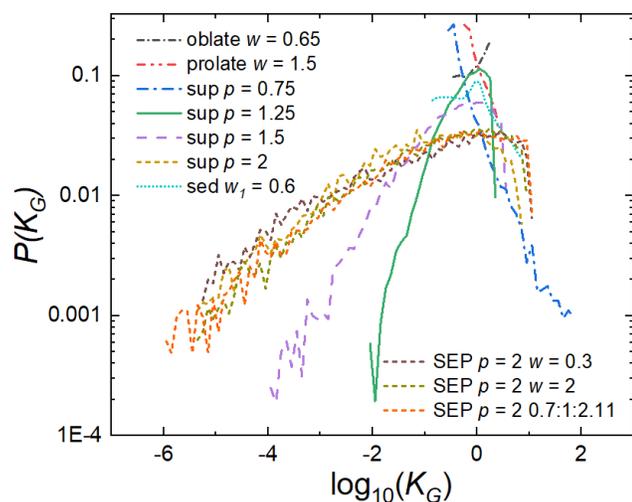
Fig. 14 Probability distribution of the scaled Gaussian curvature at each interparticle contact $P(K_G)$ in superellipsoid packings generated via Protocol 1, including oblate ellipsoids ($w = 0.65$), prolate ellipsoids ($w = 1.5$), four types of superballs ($p = 0.75$, 1.25, 1.5, and 2), self-dual ellipsoids ($w_1 = 0.6$), and three types of superellipsoids with $p = 2$ ($w = 0.3$, $w = 2$, and $w_1 = 0.7$ and $w_2 = 2.11$).

narrower and does not extend to small values of K_G.

These results suggest that contacts between flat surfaces are more likely to induce quartic modes than those between curved surfaces[53]. However, it is difficult to establish this correlation quantitatively because the vibrational modes of the dynamical matrix describe the collective behavior of all of the degrees of freedom within a jammed packing, while contact curvature only includes local geometric information[23]. Alternatively, previous studies focused on the convexity and concavity of the feasible region for constrained hard nonspherical particles in configuration space to understand hypostaticity.[17,21] A physical picture unifying these two approaches is a topic of ongoing studies.

Acknowledgements

References

1 C. S. O'Hern, S. A. Langer, A. J. Liu and S. R. Nagel, *Physical Review Letters*, 2002, **88**, 075507.

2 M. van Hecke, *Journal of Physics: Condensed Matter*, 2009, **22**, 033101.

3 G. Parisi and F. Zamponi, *Reviews of Modern Physics*, 2010, **82**, 789.

4 A. J. Liu and S. R. Nagel, *Annu. Rev. Condens. Matter Phys.*, 2010, **1**, 347–369.

5 C. Thomas and D. J. Durian, *Physical Review Letters*, 2015, **114**, 178001.

6 H. M. Jaeger, *Soft Matter*, 2015, **11**, 12–27.

7 A. V. Tkachenko and T. A. Witten, *Physical review E*, 1999, **60**, 687.

8 H. A. Makse, D. L. Johnson and L. M. Schwartz, *Physical Review Letters*, 2000, **84**, 4160.

9 W. G. Ellenbroek, E. Somfai, M. van Hecke and W. van Saarloos, *Physical Review Letters*, 2006, **97**, 258001.

10 P. Olsson and S. Teitel, *Physical Review Letters*, 2007, **99**, 178001.

11 L. Wang and N. Xu, *Soft Matter*, 2013, **9**, 2475–2483.

12 L. E. Silbert, A. J. Liu and S. R. Nagel, *Physical Review Letters*, 2005, **95**, 098301.

13 M. Wyart, L. E. Silbert, S. R. Nagel and T. A. Witten, *Physical Review E*, 2005, **72**, 051306.

14 S. Torquato and F. H. Stillinger, *Reviews of Modern Physics*, 2010, **82**, 2633.

15 G. Lu, J. R. Third and C. R. Müller, *Chemical Engineering Science*, 2015, **127**, 425–465.

16 A. Donev, I. Cisse, D. Sachs, E. A. Variano, F. H. Stillinger, R. Connelly, S. Torquato and P. M. Chaikin, *Science*, 2004, **303**, 990–993.

17 A. Donev, R. Connelly, F. H. Stillinger and S. Torquato, *Physical Review E*, 2007, **75**, 051304.

18 A. Wouterse, S. Luding and A. Philipse, *Granular Matter*, 2009, **11**, 169–177.

19 Y. Jiao, F. H. Stillinger and S. Torquato, *Physical Review E*, 2010, **81**, 041304.

20 M. Mailman, C. F. Schreck, C. S. O'Hern and B. Chakraborty, *Physical Review Letters*, 2009, **102**, 255501.

21 K. VanderWerf, W. Jin, M. D. Shattuck and C. S. O'Hern, *Physical Review E*, 2018, **97**, 012909.

22 C. F. Schreck, M. Mailman, B. Chakraborty and C. S. O'Hern, *Physical Review E*, 2012, **85**, 061305.

23 C. F. Schreck, N. Xu and C. S. O'Hern, *Soft Matter*, 2010, **6**, 2960–2969.

24 A. Wouterse, S. R. Williams and A. P. Philipse, *Journal of Physics: Condensed Matter*, 2007, **19**, 406215.

25 J. Zhao, S. Li, R. Zou and A. Yu, *Soft Matter*, 2012, **8**, 1003–1009.

26 Y. Yuan, L. Liu, W. Deng and S. Li, *Powder Technology*, 2019, **351**, 186–194.

27 T. Börzsönyi and R. Stannarius, *Soft Matter*, 2013, **9**, 7401–7418.

28 K. Asencio, M. Acevedo, I. Zuriguel and D. Maza, *Physical Review Letters*, 2017, **119**, 228002.

29 J. H. Lopez, L. Cao and J. M. Schwarz, *Physical Review E*, 2013, **88**, 062130.

30 G. W. Delaney and P. W. Cleary, *EPL (Europhysics Letters)*, 2010, **89**, 34002.

31 S. Zhao, N. Zhang, X. Zhou and L. Zhang, *Powder Technology*, 2017, **310**, 175–186.

32 Y. Yuan, L. Liu, Y. Zhuang, W. Jin and S. Li, *Physical Review E*, 2018, **98**, 042903.

33 L. Liu, Z. Yu, W. Jin, Y. Yuan and S. Li, *Powder Technology*, 2018, **338**, 67–78.

34 K. C. Smith, M. Alam and T. S. Fisher, *Physical Review E*, 2010, **82**, 051304.

35 K. C. Smith, I. Srivastava, T. S. Fisher and M. Alam, *Physical Review E*, 2014, **89**, 042203.

36 R. Ni, A. P. Gantapara, J. de Graaf, R. van Roij and M. Dijkstra, *Soft Matter*, 2012, **8**, 8826–8834.

37 R. Zou and A.-B. Yu, *Powder Technology*, 1996, **88**, 71–79.

38 A.-B. Yu, R. Zou and N. Standish, *Industrial & Engineering Chemistry Research*, 1996, **35**, 3730–3741.

39 A. Donev, F. H. Stillinger, P. Chaikin and S. Torquato, *Physical Review Letters*, 2004, **92**, 255506.

40 J. W. Perram and M. Wertheim, *Journal of Computational Physics*, 1985, **58**, 409–416.

41 T. Marschall, Y.-E. Keta, P. Olsson and S. Teitel, *Physical Review Letters*, 2019, **122**, 188002.

42 D. C. Liu and J. Nocedal, *Mathematical Programming*, 1989,

45, 503–528.

43 G. Odriozola, *The Journal of Chemical Physics*, 2012, **136**, 134505.

44 J. Veerman and D. Frenkel, *Physical Review A*, 1992, **45**, 5632.

45 B. S. John, C. Juhlin and F. A. Escobedo, *The Journal of Chemical Physics*, 2008, **128**, 044909.

46 G. W. Delaney, J. E. Hilton and P. W. Cleary, *Physical Review E*, 2011, **83**, 051305.

47 M. Neudecker, S. Ulrich, S. Herminghaus and M. Schröter, *Physical Review Letters*, 2013, **111**, 028001.

48 F. M. Schaller, M. Neudecker, M. Saadatfar, G. W. Delaney, G. E. Schröder-Turk and M. Schröter, *Physical Review Letters*, 2015, **114**, 158001.

49 K. M. Salerno, D. S. Bolintineanu, G. S. Grest, J. B. Lechman, S. J. Plimpton, I. Srivastava and L. E. Silbert, *Physical Review E*, 2018, **98**, 050901.

50 M. Trulsson, *Journal of Fluid Mechanics*, 2018, **849**, 718–740.

51 C. Song, P. Wang and H. A. Makse, *Nature*, 2008, **453**, 629.

52 L. E. Silbert, *Soft Matter*, 2010, **6**, 2918–2924.

53 J. Tian, Y. Xu, Y. Jiao and S. Torquato, *Scientific Reports*, 2015, **5**, 16722.